

Double Phase Slips and Spatio-Temporal Chaos in a Model for Parametrically Excited Standing Waves

Glen D. Granzow and Hermann Riecke

*Department of Engineering Sciences and Applied Mathematics
Northwestern University, Evanston, IL 60208, USA*

We present results of numerical simulations of coupled Ginzburg-Landau equations that describe parametrically excited waves. In one dimension we focus on a new regime in which the Eckhaus sideband instability does not lead to an overall change in the wavelength via the occurrence of a single phase slip but instead leads to “double phase slips”. They are characterized by the phase slips occurring in sequential pairs, with the second phase slip quickly following and negating the first. The resulting dynamics range from transient excursions from a fixed point resembling those seen in excitable media, to periodic solutions of varying complexity and chaotic solutions. In larger systems we find in addition localized spatio-temporal chaos, where the solution consists of a chaotic region with quiescent regions on each side. We explain the localization using an effective phase diffusion equation which can be viewed as arising from a homogenization of the chaotic state. In two dimensions the double phase slips are replaced by fluctuating bound defect pairs.

I. INTRODUCTION

Pattern formation is a striking and interesting phenomenon observed in many physical systems driven far from thermodynamic equilibrium. In addition to parametrically excited waves (which are described below), classic examples include the rolls formed in Rayleigh-Bénard convection when a fluid confined between two horizontal plates is heated from below, the annular Taylor vortices that form in a fluid between rotating concentric cylinders, and rotating spirals (and other patterns) consisting of regions of different chemical concentrations formed in chemical reactions such as the Belousov-Zhabotinsky reaction. A review of pattern forming systems can be found in [1]. Typically, the basic equations that describe these pattern-forming experiments are quite complicated (such as the Navier Stokes equations). However, for pattern-forming systems near onset, the complicated system of equations can often be simplified using asymptotic expansions for small amplitudes. The resulting amplitude equations (e.g. [2–5]) describe the variation of the pattern on large space and time scales.

In many systems transitions from simple to chaotic behavior are found when a control parameter (such as the temperature difference in Rayleigh-Bénard convection, the angular velocity of the inner cylinder in Taylor-Couette flow, or the supplied concentration of a particular chemical in a reaction diffusion system) is changed. Studies of chaos began with low-dimensional attractors as found, for instance, in the Lorentz system [6] and have progressed to chaotic behavior in both space and time in spatially extended systems with a large number of degrees of freedom. Of particular interest in both experimental and mathematical systems is identifying features that allow the different types of observed chaos to be classified in some way. A well studied example is the complex Ginzburg-Landau equation, for which a number of different chaotic regimes have been identified [7–11]. Relevant for the present paper is the observation that a distinction can be drawn between a phase-chaotic regime and amplitude-chaotic ones. In one dimension amplitude chaos is characterized by the occurrence of phase slips during which the amplitude of the wave goes to zero and the total phase of the system changes by 2π , that is, a wavelength is inserted or eliminated. In phase chaos there are essentially no phase slips [9,11] and the system can be described by an equation for the phase of the wave alone [12]. For the complex Ginzburg-Landau equation this phase equation is the Kuramoto-Sivashinsky equation. Phase equations break down during phase slips so they cannot be used to describe amplitude chaos.

In this paper we consider parametrically excited waves, which are also a classic pattern forming system [13]. Parametrically excited waves arise quite generally in systems exhibiting weakly damped modes that are oscillatory in both space and time, when these modes are forced at twice their natural frequency. Faraday’s experiment [13] in which surface waves are formed on a liquid in a vertically oscillated container is probably the most well known example. Stripe, square, and hexagon patterns (e.g. [14]), as well as quasipatterns [15], spirals [16], and chaotic states (e.g. [17,18,14]) have all been observed in Faraday experiments with various fluids, forcing amplitudes, and frequencies. Parametrically excited waves have also been observed in magnetic materials (spin waves) [19,20], in electroconvection in nematic liquid crystals [21,22], and in Taylor-Dean flow [23].

In this paper we discuss dynamics arising in numerical simulations of a system of equations that model parametrically excited waves and focus on solutions which are chaotic in space and time. In our simulations we find chaotic solutions which are characterized by a new phenomenon: double phase slips in one dimension and the analogous bound defect pairs in two dimensions. These phenomena are described in sections III and VI. In addition to chaotic solutions where

these phenomena occur irregularly in space and time, which are described in sections IV C and V A, we also describe transient and periodic solutions involving double phase slips in sections IV A and IV B.

Of central interest in our one-dimensional simulations are localized chaotic states (section V B). That is, there are solutions that include a spatial region, bounded by quiescent regions on each side, in which the dynamics are irregular in space and time. Experimentally, similar phenomena have been observed in Taylor vortex flow [24], Rayleigh-Bénard convection [25], and parametrically excited surface waves [18,14]. The localization mechanism in these experimental systems is only poorly understood. For the system of equations discussed in this paper the localization can be understood using an effective phase diffusion equation. We confirm the validity of this approach by explicitly determining the effective phase diffusion coefficient in section V C. A short account of these results has been presented previously [26].

While most of the results in this paper are for a one dimensional system, section VI describes results for an analogous system in two dimensions. Section VII concludes our paper with a summary and discussion of the results.

II. THE MODEL

The equations we consider in this paper generically describe a system with a uniform state that has a supercritical Hopf bifurcation to a state that is periodic in both space and time when subjected to a uniform, constant forcing. Subjecting the system to an additional spatially uniform, time-periodic forcing at approximately twice the Hopf frequency creates a codimension-three bifurcation point involving the following three parameters: 1) the amplitude of the time-independent forcing, 2) the amplitude of the periodic forcing, and 3) the frequency of the periodic forcing. In the vicinity of this codimension-three bifurcation point the following amplitude equations [27–29] are derived by considering the reflection and translation symmetries in space and the weakly broken translation symmetry in time:

$$\partial_T A + s\partial_X A = d\partial_X^2 A + aA + bB + cA(|A|^2 + |B|^2) + gA|B|^2, \quad (1)$$

$$\partial_T B - s\partial_X B = d^*\partial_X^2 B + a^*B + bA + c^*B(|A|^2 + |B|^2) + g^*B|A|^2. \quad (2)$$

The dependent variables A and B are complex, and represent amplitudes of left and right traveling waves that are summed together to yield the solution of the underlying system:

$$u(x, t) = \epsilon A(X, T)e^{i(q_c x - \frac{\omega_c}{2} t)} + \epsilon B(X, T)e^{i(q_c x + \frac{\omega_c}{2} t)} + c.c. + o(\epsilon), \quad (3)$$

where $u(x, t)$ would give, for example, the position of the fluid surface in the Faraday experiment. The amplitudes A and B vary on the slow time and space scales, $T = \epsilon^2 t$ and $X = \epsilon x$. The coefficients in (1,2) are complex except for s and b , which are real. The real part of the coefficient of the linear term a gives the linear damping of the traveling waves in the absence of the periodic forcing and is proportional to the distance from the Hopf bifurcation. The coefficient of the linear coupling term b gives the amplitude of the periodic forcing. (Note that this term breaks the time translation symmetry.) The imaginary part of the coefficient of the linear term a gives the difference between the frequency of the unforced waves and half the forcing frequency ω_e .

While in general a codimension-three bifurcation might be difficult to realize in an experiment, in the above situation (involving a system that undergoes a Hopf bifurcation) each of the three bifurcation parameters are natural control parameters in the system. In the Faraday experiment, however, there is no Hopf bifurcation and the above equations are only valid in the limit of weak damping (small viscosity). In this case the coefficients of the nonlinear terms c and g would be purely imaginary, since their real parts also represent (nonlinear) damping and would be higher order. In addition, for the Faraday experiment the group velocity parameter s would generally be complex, and s in (2) would be replaced by its complex conjugate s^* .

There is one caveat concerning (1,2) when they are used to describe either the Faraday experiment or parametrically excited waves induced near a Hopf bifurcation point. With the scaling $X = \epsilon x$, the group velocity term (involving ∂_X) would generically appear at lower order, so (1,2) require that the group velocity is small. If it is not small a strict asymptotic analysis would require the introduction of a second slow time scale and would lead to equations in which the cross-coupling between A and B arises through a spatially averaged term [30–34].

Note that (1,2) are in one (spatial) dimension. With periodic boundary conditions (as will be imposed in our numerical simulations) these equations would describe (for example) the Faraday experiment in an annular container. Equations in two (spatial) dimensions (see (27,28) below) are discussed in section VI.

Solutions of (1,2) of the form $A = A_0 e^{iQX}$, $B = B_0 e^{iQX}$ include those where A_0 and B_0 are constants of unequal magnitude that correspond to traveling waves in the underlying system (see (3)), and those where A_0 and B_0 are constants with equal magnitude that correspond to standing waves in the underlying system [27,28]. It is these standing-wave solutions, which are phase locked to the periodic forcing, that are the focus of this paper. In particular,

we discuss the ensuing dynamics when these standing waves are perturbed. There are also solutions where A_0 and B_0 have equal magnitude but vary periodically in time, which correspond to standing waves that are not phase locked to the external forcing [27]. We do not treat these standing waves in this paper.

The standing waves which are phase locked to the external forcing are stationary solutions of (1,2) and are given by [27,28]

$$A = R e^{i(QX + \phi_A)} \quad (4)$$

$$B = R e^{i(QX + \phi_B)} \quad (5)$$

$$\text{where: } R^2 = \frac{-(\hat{a}_r n_r + \hat{a}_i n_i) \pm \sqrt{(\hat{a}_r n_r + \hat{a}_i n_i)^2 - (n_r^2 + n_i^2)(\hat{a}_r^2 + \hat{a}_i^2 - b^2)}}{(n_r^2 + n_i^2)} \quad (6)$$

$$\phi_B - \phi_A = \arctan \frac{\hat{a}_i + n_i R^2}{\hat{a}_r + n_r R^2} \quad (7)$$

$$\text{and: } \hat{a} \equiv \hat{a}_r + i\hat{a}_i = a - isQ - dQ^2 \quad (8)$$

$$n \equiv n_r + in_i = 2c + g. \quad (9)$$

They arise from the trivial solution in a steady bifurcation at the onset $b^2 = \hat{a}_r^2 + \hat{a}_i^2$. Equations (4,5) actually give a family of solutions for each wavenumber Q since the phase ϕ_A (or ϕ_B) can be chosen arbitrarily. Changing the value of ϕ_A (with $\phi_B - \phi_A$ fixed) corresponds to spatial translations of the solution.

Close to onset (1,2) can be reduced to a single Ginzburg-Landau equation with real coefficients [35]. This implies that the waves are stable near onset in a band of wavenumbers which is limited by the Eckhaus (i.e. a long-wavelength) instability. Near onset the neutral and Eckhaus curves are parabolic [36]. For larger values of the forcing amplitudes b , the Eckhaus curve need no longer be parabolic and can assume a variety of shapes. For $a = -0.05$, $c = -1 + 4i$, $d = 1 + 0.5i$, $s = 0.2$, $g = -1 - 12i$, the Eckhaus curve closes on itself as shown in Figure 1 [35]. Thus, for $b > 0.85$ all standing waves become unstable, somewhat reminiscent of the Benjamin-Feir instability of traveling waves [37]. In this paper we focus on the dynamics resulting from the Eckhaus instability. All computations presented in this paper were made using the same parameter values as used in Figure 1.

In reference [35] the Eckhaus curve in Figure 1 was obtained using phase dynamics. A more complete linear stability analysis considering sideband perturbations with arbitrary wavenumbers confirms that there is no short-wavelength instability for these parameter values.

III. PHASE SLIPS AND DOUBLE PHASE SLIPS

The main questions to be addressed in this paper are: What are the solutions to (1,2) if started with initial conditions that correspond to unstable standing waves? What features characterize the solutions? How do the solutions differ as one changes the forcing amplitude b and the wavenumber of the initial condition Q ? We investigate these questions by calculating numerical approximations to the solutions of (1,2) using a pseudospectral method in space (periodic boundary conditions) and a fourth-order Runge-Kutta/integrating-factor scheme in time.

The dynamics described in this paper all incorporate a feature we call a ‘‘double phase slip’’. In this section we describe this feature and contrast it to an ordinary single phase slip, which is a well known feature of many systems (including the solution of a single Ginzburg-Landau equation with real coefficients) when started with an initial condition that is Eckhaus unstable. In order to excite the Eckhaus instability we typically choose an initial condition that is a wave, perturbed so that the local wavenumber varies slightly throughout the domain such that it has a maximum and a minimum at distinct locations.

Since near onset (1,2) can be reduced to a single real Ginzburg-Landau equation [35], the solution of (1,2) for small values of b should resemble the solution of a single real Ginzburg-Landau equation. This is indeed seen in our simulations. For small values of b ($b = 0.1$, say) and an initial condition slightly to the right of the Eckhaus stable region in Figure 1, the solution undergoes a phase slip near the location of the initial maximum in the wavenumber that reduces the wave number and moves the solution into the stable region. This behavior is shown in Figure 2a. For larger values of b however ($b = 0.6$, say), the behavior of the solution is markedly different, as shown in Figure 2b; given an initial condition slightly to the right of the Eckhaus stable region, the solution undergoes a phase slip that reduces the average wave number but a short time later undergoes a second phase slip at essentially the same location in space that restores the wave number to its original value. This *double phase slip* causes the solution to remain in the Eckhaus unstable region, thus allowing persistent dynamics.

In our simulations a phase slip in A is always accompanied by an essentially coincident phase slip in B . Thus when we refer to a double phase slip in the solution of (1,2) we mean that there are double phase slips in both A and B at approximately the same point in space and time.

Double phase slips occur in a variety of solutions to (1,2) including periodic solutions, chaotic solutions, and non-trivial transients. These solutions are described in the following sections. We first present results for small system sizes. Then we discuss large systems and show that they allow a simplified long-wave description.

IV. DYNAMICS OF A SMALL SYSTEM

For the simulations presented in this section the domain size L has been chosen such that the initial conditions, which have an average wave number in the vicinity of the Eckhaus curve, include only five wavelengths. Three different types of solutions are presented: 1) Transient solutions where there is only a single double phase slip, 2) Solutions where double phase slips occur periodically in time, and 3) Complex solutions where double phase slips occur irregularly in space and time. Figure 3 shows where examples of these solutions occur in relation to the Eckhaus curve that is shown in Figure 1. The initial conditions for these solutions are close to the standing wave solutions but perturbed such that there is a maximum in the local wave number that triggers the first double phase slip and determines its location. Examples of each of the solution types are described below.

A. Transient Solutions

In the transient solutions described here, there is only one double phase slip. After the double phase slip, the solution relaxes to the stationary solution corresponding to the regular standing wave state in the underlying system. These transient solutions resemble the response of an excitable medium; beginning with an initial condition that is in the vicinity of a stable fixed point, the transient solution makes an excursion far away from the fixed point before finally coming to rest there. This is most clearly seen in the phase-plane representation of the solution shown in Figure 4. It shows the magnitudes of the (spatial) Fourier modes corresponding to 4 and 5 wavelengths in the domain. Each dot in Figure 4 represents an instant in time. The square indicates the initial condition which is the perturbed 5-wave state. The loop in Figure 4 is traversed once, with the final state of the solution being the fixed point on the vertical axis (marked by a diamond) corresponding to the (stable) 5-wave solution.

Solutions with a single double phase slip occur only where the initial condition is a perturbation of a *stable* solution. The lowest point on Figure 3 appears to contradict this statement since it appears on the outside of the Eckhaus curve. However, this is due to the fact that the Eckhaus curve represents a long-wavelength instability. Since arbitrarily small wavenumbers are not present in our finite domain the true stability curve for our finite system is slightly outside the Eckhaus curve and all of the solutions with a single double phase slip are in fact within the stable region. At the stability limit an unstable saddle-point solution branches subcritically off the branch of solutions given by (4-9) [38,39]. The perturbation required to excite a double phase slip must place the initial condition beyond this saddle point in phase space. As the wavenumber is moved further into the Eckhaus stable region, the bifurcated saddle point moves further from the stable stationary solution in phase space, and a larger perturbation is required to excite the system.

B. Periodic Solutions

In the periodic solutions, double phase slips occur at the same locations in space, periodically in time. An example of the simplest of these periodic solutions is shown in Figure 5 where the location in space and time of each double phase slip is indicated by a circle. The time between each double phase slip is much larger than the time between the individual phase slips which make up a double phase slip. This can be appreciated by looking at Figure 6 which shows the (spatial) average of the wavenumber plotted versus time. Each of the downward “spikes” in Figure 6 represents a double phase slip; the average wavenumber is reduced by the first phase slip, then restored by the second. Figure 7 shows the phase-plane representation of the simple periodic solution. The loop in Figure 7 is traversed periodically, with the upper left portion of the loop (where the mode 5 magnitude is large and the mode 4 magnitude is small) being passed between double phase slips, and the lower right portion of the loop (where the mode 5 magnitude is smaller and the mode 4 magnitude is larger) being passed during a double phase slip.

Although the periodic solutions occur for larger wavenumbers (for a given value of b) than the transient solutions where there is only one double phase slip (see Figure 3) we find that the periodic solutions can still occur within the Eckhaus stable region indicating that stable stationary solutions and stable periodic solutions can coexist.

As the wavenumber is decreased the period of the simple periodic solutions diverges as shown in Figure 8. This appears to be due to the unstable saddle-point solution which branches subcritically off the branch of solutions given

by (4-9) at the Eckhaus stability limit. Inside the Eckhaus stable region, as the average wavenumber of the initial condition is decreased by increasing the size of the system L , the saddle point moves away from the stable fixed point and towards the periodic orbit in phase space. This causes the periodic orbit to pass closer to the saddle point, increasing its period (cf. Figure 8). Our simulations suggest that the divergence of the period occurs when the periodic orbit becomes a homoclinic orbit of the saddle point. Beyond this point the periodic solutions no longer exist and the excitable transient solutions occur.

Increasing the wavenumber from those which produce simple periodic solutions we find a period doubling bifurcation which leads to the solution shown in Figure 9. Increasing the wavenumber further results in even more complicated periodic (or quasiperiodic) states such as that shown in Figure 10 where a wave of double phase slips propagate through the system. The exact form of the more complicated periodic solutions may depend on the value of b but the trend of simple periodic solutions losing stability to more complicated periodic solutions was observed for all investigated values of b that exhibit periodic solutions.

C. Complex Solutions

Figure 11 shows a complex solution where the double phase slips occur irregularly in space and time. The complex solutions occur for even larger wavenumbers (for a given value of b) than the periodic solutions. If the average wave number of the initial condition is too large however, a single phase slip occurs, which reduces the wavenumber. The phase slip need not take the solution all the way into the stable band. Instead the solution can remain in the domain of periodic or even complex dynamics.

V. DYNAMICS OF A LARGE SYSTEM

In this section we present solutions for larger domains than the solutions discussed in the previous section. For the particular solutions discussed, approximately 50 wavelengths with a wavenumber near the Eckhaus curve fit in the domain whereas in the previous section only 5 did. We focus on the complex solutions where the double phase slips occur irregularly in space and time. Based on the irregular appearance of these solutions we believe them to be chaotic. Autocorrelation functions calculated using the location of the double phase slips show that these locations are not correlated for large distances and times, confirming the chaotic nature of the solutions in both space and time. We discuss two different solution types: 1) Extended spatio-temporal chaos where the double phase slips occur irregularly across the entire domain, and 2) Localized spatio-temporal chaos where the irregular occurrence of double phase slips is restricted to only part of the spatial domain.

A. Extended Spatio-Temporal Chaos

Figure 12a shows a space-time diagram similar to Figure 11 for an extended chaotic solution in a large system, with each double phase slip represented by a single dot. The extended chaotic states exist over a range of wavenumbers with the space-time density of double phase slips increasing with wavenumber as seen in Figure 12b. Beyond a certain wavenumber the chaotic state loses stability, however. A solution with such a large initial wavenumber is represented in Figure 12c where at $t \approx 13000$ and $x \approx 265$ a *single* phase slip occurs, which reduces the local wavenumber. Subsequently there are no phase slips in this area until the higher wavenumber in the regions on either side diffuses in. Eventually the wavenumber and the density of double phase slips in Figure 12c become homogeneous again and their final values are the same as those in Figure 12b. The transition appears to be related to the fact that with the large wavenumber (that is, before the single phase slip in Figure 12c) the time between the occurrence of double phase slips at a given location in space is similar to the duration of each double phase slip, i.e. the time between the two phase slips within a double phase slip. This is due to both the high density of double phase slips and their tendency to reoccur at the same location in space.

B. Localized Spatio-Temporal Chaos

Perhaps the most interesting solutions arising in our simulations are those featuring localized spatio-temporal chaos. An example is shown in Figure 13. As in Figure 12, each double phase slip is represented by a single dot. We start with an initial condition with a maximum in the local wavenumber that triggers an initial double phase slip. This

initial double phase slip triggers additional double phase slips in the vicinity of the first. Originally the size of the region in which the double phase slips occur grows with time. However, for later time, the size of the region ceases to grow and the chaos is seen to be localized. Outside of the region in which the double phase slips occur, the solution is the time-independent solution which corresponds to standing waves in the underlying system.

Figure 14 shows the width of the chaotic region as a function of time for different initial widths bracketing the final width of the state shown in Figure 13. For both initial conditions the width converges to the same final value indicating that in the final state the spatio-temporal chaos is indeed localized.

C. Effective Phase Equation

The localization mechanism for the steady and chaotic regions in Figure 13 can be understood using an effective phase diffusion equation. In this section we present this analysis. Our analysis uses the phase of $A(X, T)$ but an analysis based on $B(X, T)$ would yield the same results.

From our investigation of solutions with extended chaos we expect the chaotic region to have a larger local wavenumber than the region where the solution is time independent (see Figure 3). Figure 15 shows the local wavenumber of the time average of the solution $A(X, T)$ (averaged from $t = 2,000,000$ to $t = 2,010,000$) for the state represented in Figure 13 and confirms this; the local wavenumber in the chaotic region is larger than the local wave number in the quiescent region. The local wavenumber for $B(X, T)$ is similar. So the steady and chaotic regions in Figure 13 can be viewed as domains with differing wavenumber.

Somewhat similar stationary states consisting of domains of differing wavenumber have been observed experimentally in convection in narrow channels [40], as well as in Taylor vortex flow [24] and in two-dimensional optical patterns [41]. The convection states can be described by the phase diffusion equation¹ [44,35,42,43]

$$\partial_T \phi(X, T) = D(q) \partial_X^2 \phi(X, T) + h.o.t., \quad (10)$$

which is nonlinear due to the dependence of D on $q \equiv \partial_X \phi$. The higher order terms include higher derivative terms (e.g. $G \partial_X^4 \phi(X, T)$) which are important when D is small or negative, or when these higher derivatives are large. Stable solutions of (10) that consist of domains of differing wavenumber can occur if the diffusion coefficient $D(q)$ is negative only over a small range of wavenumbers. In this situation, initial conditions with a uniform wavenumber in this unstable range will evolve to a structure consisting of domains in which the local wavenumber lies in either of the two adjacent ranges of stable wavenumbers. At the interface between these domains, the higher-order terms in (10) are important and there is an internal transition layer (similar to a boundary layer). These transition layers can be studied using matched asymptotic expansions as has been done for the Cahn-Hilliard equation and other related equations similar to (10) [45].

Equation (10) is only valid as long as the gradients in the wavenumber are small. During phase slips this is not the case. In fact, the phase ϕ is not even defined at one instant during the phase slip process. The solution shown in Figure 13 includes phase slips and thus cannot be described by (10). However, because each phase slip in the solution in Figure 13 is immediately followed by a second phase slip which restores the phase to its value before the first phase slip, on a long time scale the effective total phase $\Delta \hat{\phi} = \int_0^L \hat{q} dX$ of the system is conserved. Here the effective wavenumber \hat{q} is defined to be $\partial_X \hat{\phi}$ where $\hat{\phi}$ is the phase of a running time average of $A(X, T)$:

$$\hat{A}(X, T) = \frac{1}{\Delta T} \int_{T-\Delta T}^{T+\Delta T} A(X, T) dT \equiv \hat{R} e^{i\hat{\phi}}. \quad (11)$$

The time interval ΔT is chosen so that (11) averages over many double phase slips. An equivalent analysis could also be based on the phase of a running time average of $B(X, T)$ instead of $A(X, T)$. The $A(X, T)$ portion of the solution to (1,2) can be written as

$$A(X, T) = \hat{A}(X, T) + F_A(X, T) \quad (12)$$

where $F_A(X, T) \equiv A(X, T) - \hat{A}(X, T)$ contains the rapid fluctuations due to the phase slips and has small magnitude except in the neighborhood of a phase slip. $\hat{A}(X, T)$ contains variations on slower time and space scales and we

¹Certain phenomena such as the locking of adjacent domain walls into each other are not captured by the phase equation (10). For small amplitudes of the pattern the locking can be described by suitable Ginzburg-Landau equations [42,43].

assume that $\hat{R} = \hat{R}(\hat{q})$ (this is similar to (6)). Due to the translation symmetry in time and translation and reflection symmetries in space of (1,2), the long-wave evolution equation for the effective phase $\hat{\phi}(X, T)$ is expected to be a diffusion equation similar to (10)

$$\partial_T \hat{\phi}(X, T) = \hat{D}(\hat{q}) \partial_X^2 \hat{\phi}(X, T) + h.o.t.. \quad (13)$$

In order to test this explicitly, we measure the effective phase diffusion coefficient \hat{D} by measuring the response of the effective phase of the chaotic state to a localized time-periodic forcing. This approach to measuring the effective diffusion coefficient of a chaotic state is similar to that used in experiments on turbulent Taylor vortex flow wherein an endcap was moved sinusoidally [46]. Perhaps it should be emphasised that, while we want to measure the effective diffusion coefficient to understand the localized chaotic states (as shown in Figure 13), the actual measurements described in this section are done on extended chaotic states (as shown in Figure 12). Localized forcing of the effective phase in our simulations is accomplished by including a spatially local, time-periodic advection term in (1,2) giving:

$$\partial_T A + (v + s) \partial_X A = d \partial_X^2 A + aA + bB + cA(|A|^2 + |B|^2) + gA|B|^2 \quad (14)$$

$$\partial_T B + (v - s) \partial_X B = d^* \partial_X^2 B + a^* B + bA + c^* B(|A|^2 + |B|^2) + g^* B|A|^2 \quad (15)$$

$$\text{with } v = \begin{cases} v_0 \sin(\omega_0 T) & \text{for } X_1 \leq X \leq X_2 \\ 0 & \text{otherwise.} \end{cases}$$

For small values of v_0 and ω_0 , the localized advection term causes formerly stationary solutions to drift within the region $X_1 \leq X \leq X_2$, periodically reversing their direction according to the sign of v . For the regions $X < X_1$, and $X > X_2$ the situation resembles an imposed boundary condition at $X = X_1$, and $X = X_2$ at which the phase of the solution varies sinusoidally.

The solution to (13) for $X > X_2$, which satisfies the boundary condition $\hat{\phi}(X_2, T) = \epsilon \sin(\omega_0 T)$, is

$$\hat{\phi}(X, T) = \hat{Q}_0(X - X_2) + \epsilon e^{-\alpha(X - X_2)} \sin(\omega_0 T - \beta(X - X_2)) \quad (16)$$

$$\text{where } \alpha = \beta = \sqrt{\frac{\omega_0}{2\hat{D}}}. \quad (17)$$

If the effective phase of the solution $A(X, T)$ in the region $X > X_2$ obeys this relationship we have

$$\hat{A}(X, T) = \hat{R} e^{i\hat{\phi}(X, T)} = \hat{R} e^{i(\hat{Q}_0(X - X_2) + \tilde{\phi})} \quad (18)$$

$$\text{where } \tilde{\phi} = \epsilon e^{-\alpha(X - X_2)} \sin(\omega_0 T - \beta(X - X_2)) \quad (19)$$

$$\text{and } \hat{R} = \hat{R}(\partial_X \hat{\phi}(X, T)) = \hat{R}(\hat{Q}_0 + \partial_X \tilde{\phi}). \quad (20)$$

If v_0 and ω_0 are small then the magnitude of the periodic variations in the effective phase $\tilde{\phi}$ will also be small. Taylor expanding $\hat{R}(\hat{Q}_0 + \partial_X \tilde{\phi})$ and $e^{i\tilde{\phi}}$ gives

$$\hat{A}(X, T) \sim (\hat{R}(\hat{Q}_0) + \hat{R}'(\hat{Q}_0) \partial_X \tilde{\phi} + \dots) e^{i\hat{Q}_0(X - X_2)} (1 + i\tilde{\phi} + \dots). \quad (21)$$

Taking the Fourier transform of $A(X, T)$ in time,

$$\mathcal{A}(X, \Omega) = \frac{1}{\tau} \int_0^\tau e^{i\Omega T} A(X, T) dT = \frac{1}{\tau} \int_0^\tau e^{i\Omega T} \hat{A}(X, T) dT + \frac{1}{\tau} \int_0^\tau e^{i\Omega T} F_A(X, T) dT, \quad (22)$$

and assuming that the fast variations $F_A(X, T)$ give only negligible contributions to the Fourier components at low frequencies yields

$$\mathcal{A}(X, -\omega_0) \approx \frac{\epsilon}{2} \left[(\hat{R}(\hat{Q}_0) - \beta \hat{R}'(\hat{Q}_0)) + i\alpha \hat{R}'(\hat{Q}_0) \right] e^{-\alpha(X - X_2) + i(\hat{Q}_0 - \beta)(X - X_2)} \quad (23)$$

$$\mathcal{A}(X, \omega_0) \approx \frac{\epsilon}{2} \left[(-\hat{R}(\hat{Q}_0) - \beta \hat{R}'(\hat{Q}_0)) - i\alpha \hat{R}'(\hat{Q}_0) \right] e^{-\alpha(X - X_2) + i(\hat{Q}_0 + \beta)(X - X_2)}. \quad (24)$$

Thus, the magnitude of the Fourier modes $\mathcal{A}(X, -\omega_0)$ and $\mathcal{A}(X, \omega_0)$ (corresponding to the frequency ω_0 in the localized advection term) will decay exponentially in space as $X - X_2$ increases if the phase behaves diffusively. Figure 16 shows that this exponential behavior is realized in our simulations. It gives the absolute value of the Fourier mode $\mathcal{A}(X, \omega_0)$ versus space for two different values of the frequency ω_0 . According to (17) the decay rate α is proportional

to $\omega_0^{1/2}$ for diffusive behavior. The ratio of the slopes of the curves in Figure 16 are consistent with this diffusive scaling. Note that for larger frequencies, and therefore larger gradients of $\hat{\phi}$, higher order terms (like $-\hat{G}\partial_X^4\hat{\phi}$, etc.) have to be kept in the diffusion equation which affect the dependence on ω . For $\hat{G} > 0$, α is expected to go to zero slower than $\omega^{1/2}$:

$$\frac{\alpha(\omega_1)}{\alpha(\omega_2)} = \left(\frac{\omega_1}{\omega_2}\right)^{1/2} \left[1 + \frac{\hat{G}}{2\hat{D}^2}(\omega_2 - \omega_1) + O(\omega_1\omega_2)\right]. \quad (25)$$

We found analogous behavior in the nonchaotic regime where our simulations were able to reproduce the analytical value of the diffusion coefficient.

The phase slips introduce noise which can be seen in Figure 16. In order to reduce the effect of this noise and extract a reliable decay rate α , the Fourier integral (22) has been extended over many periods ($\tau = 88 \times 2\pi/\omega_0$) of the function $v(X, T)$ in the advection term in (14,15).

From the decay rate α we can calculate the diffusion coefficient \hat{D} using (17). We can also calculate \hat{D} using β which is obtained from the ratio of the Fourier coefficients $\mathcal{A}(X, \omega_0)$ and $\mathcal{A}(X, -\omega_0)$ given by (23,24):

$$\log\left(\frac{\mathcal{A}(X, \omega_0)}{\mathcal{A}(X, -\omega_0)}\right) = \log\left(\frac{(-\hat{R}(\hat{Q}_0) - \beta\hat{R}'(\hat{Q}_0)) - i\alpha\hat{R}'(\hat{Q}_0)}{(\hat{R}(\hat{Q}_0) - \beta\hat{R}'(\hat{Q}_0)) + i\alpha\hat{R}'(\hat{Q}_0)}\right) + i2\beta X. \quad (26)$$

A plot of the imaginary part of this quantity versus X will be linear with slope 2β if the effective phase is behaving diffusively. Figure 17 shows this plot for the same simulations as presented in Figure 16 and exhibits the expected linear behavior near X_1 and X_2 .

The diffusion equation (13) yields $\alpha = \beta$ (cf. (17)) so the slopes indicated on Figure 17 should be twice those indicated on Figure 16. Although the small discrepancies could be due to higher order terms in (13) they are within the margin of error in the measurement which is mainly due to the short-scale chaotic dynamics.

We conclude from the results in Figures 16 and 17 that the dynamics of the effective phase are indeed diffusive and show in Figure 18 the wavenumber dependence of the effective phase diffusion coefficient $\hat{D}(\hat{q})$ along with the analytical phase diffusion coefficient for the stationary solution [35]. The solid curve shows the analytical phase diffusion coefficient D for the stationary solution. The triangles give the effective phase diffusion coefficient \hat{D} for the chaotic solutions as measured by using the decay rate α , while the circles show \hat{D} as measured using β . Despite the scatter in the data it is clear that $\hat{D}(\hat{q})$ decreases with decreasing \hat{q} and presumably goes to zero at a wavenumber for which the diffusion coefficient of the nonchaotic state is still negative as shown by the dashed line. Thus the phase of the system is diffusively unstable over a finite range of wavenumbers. This, along with the conservation of the total phase (here the conservation of the total *effective* phase), is known to lead to stable domains of differing wave numbers, and explains the localization of the chaotic region in Figure 13.

For the wavenumbers at which we were able to measure the effective diffusion coefficient, the effective phase of the solution remains almost stationary in the absence of any localized forcing. For larger wavenumbers, however, the effective phase drifts significantly on the time scale over which we attempted to make our diffusion coefficient measurements. Because of this we were unable to measure the effective diffusion coefficient for larger wavenumbers than those included in Figure 18.

Figure 18 suggests that the chaotic activity should not disappear homogeneously if the average wavenumber is decreased towards the stable regime. Instead, the homogeneously chaotic state should become unstable to long-wave modulations and eventually split up into chaotic and stationary domains in which the local wavenumber is in the respective stable regimes ($D > 0$ and $\hat{D} > 0$). A similar breaking up of the homogeneous state is expected as the forcing amplitude b is increased. Numerical simulations confirm this as shown in Figure 19.

VI. THE TWO DIMENSIONAL PROBLEM

In this section we consider a two-dimensional version of (1,2)

$$\partial_T A + s\partial_X A = d\partial_X^2 A + d_2\partial_Y^2 A + aA + bB + cA(|A|^2 + |B|^2) + gA|B|^2 \quad (27)$$

$$\partial_T B - s\partial_X B = d^*\partial_X^2 B + d_2^*\partial_Y^2 B + a^*B + bA + c^*B(|A|^2 + |B|^2) + g^*B|A|^2 \quad (28)$$

These equations describe parametrically excited waves in a two-dimensional *anisotropic* system. The usual Faraday experiment is *not* described by these equations since it is isotropic. An experimental system that *is* described by (27,28) is electroconvection in nematic liquid crystals [21], in which the anisotropy is due to a preferred direction of

the rod-like molecules. Parametrically excited waves have been observed in both the normal roll regime [21], in which the waves are perpendicular to the preferred direction of the molecules, and in the oblique roll regime [22], in which the waves are at an oblique angle to the preferred direction. The normal rolls are described by (27,28) while the oblique rolls are described by *four* coupled amplitude equations [47].

The linear stability analysis of the standing wave solution of (27,28) must consider perturbations transverse to the waves as well as along them. This allows additional instabilities as compared to the one-dimensional case. For the parameters chosen for the one-dimensional simulations above, along with the dispersion coefficient in the y -direction $d_2 = d$, a stable wavenumber band exists for $0.05 < b < 0.85$.

As in the one-dimensional case (27,28) can be reduced to a single Ginzburg-Landau equation with real coefficients near onset. Therefore the solutions for small b are similar to those of a single real Ginzburg-Landau equation and the solution with an initial condition slightly outside the Eckhaus stability limit undergoes a transition which reduces the wavenumber. In two dimensions the transition from an Eckhaus unstable wave number to a stable wave number involves the creation of defect pairs which are created together and then move apart as shown in Figure 20. There, part of the spatial domain of the problem at eight sequential times is represented by the eight squares. Within each square the solid curves represent locations where the real part of the solution is zero, and the dashed curves represent locations where the imaginary part of the solution is zero. Locations where a solid curve crosses a dashed curve are the “defects” where the amplitude of the solution is zero. These defects are indicated by circles in Figure 20. The defects, which form as a pair (at some $500 < t < 600$ in Figure 20), move apart leaving one less wave in the domain after they have moved far apart ($t = 2500$). This is analogous to a phase slip in one dimension.

For larger values of b the solutions to (27,28) also involve the creation of defect pairs. However, the defects often do not move far apart but stop after separating some finite distance, turn around and annihilate each other. This can be visualized by considering only the left column of Figure 20. The solution begins with the downward sequence of squares from the top as sequential in time (as in the standard Eckhaus transition). However, on reaching the bottom of the column ($t = 650$) the time sequence reverses and leads back to the top of the column where the wavenumber resumes its original value. Such a *bound defect pair* is analogous to a *double* phase slip in one dimension. In our two-dimensional simulations we have not found the single bound defect pair or simple periodic solutions that are suggested by this visualization. But we have seen solutions where many of the defects which are created together as pairs annihilate each other. Figure 21 is a space-time diagram of such a solution for $b = 1.2$. The spatial aspect of Figure 21 is a projection; the y coordinate is not represented. Each circle represents the x -coordinate of the position of a defect and the time it was at this location. Small and large circles denote defects of opposite polarity (as they do in Figure 20). Focusing on the “bubble” formed by the pair of defects created at $x \approx 29$ and $t \approx 2680$ we see that the defects in this pair indeed move apart for a short time before they reverse their directions, ultimately annihilating each other at $x \approx 30$ and $t \approx 2710$. There are many such bubbles on the diagram as well as more complex events such as bubbles involving two or three defect pairs. While for this value of b most defects are “bound” in such a bubble, there are also a few isolated “unbound” defects as well. In these preliminary calculations we have not investigated the statistics of bound and unbound defects and the dependence of the statistics on the forcing amplitude b .

Figures 20 and 21 are based on $A(X, Y, T)$. Similar to the phase slips in the one-dimensional problem, in our two-dimensional simulations a defect in A is always accompanied by a defect in B at a nearby location.

VII. CONCLUSIONS AND DISCUSSION

We have presented numerical solutions of a pair of coupled Ginzburg-Landau equations that are amplitude equations for parametrically excited waves ((1,2),(27,28)). In particular, we have studied the ensuing dynamics when solutions of these equations corresponding to standing waves which are phase locked to the external forcing are perturbed. Parameters in the equations were chosen such that there is a forcing amplitude above which all wave numbers are linearly unstable (Figure 1). The usual transition from an Eckhaus-unstable state to a stable state (Figures 2a, 20) is found near onset but not for larger forcing amplitudes.

In one dimension *double phase slips* (Figure 2b) occur with these larger forcing amplitudes. These double phase slips allow periodic dynamics with an average wavenumber that is Eckhaus unstable even for parameters for which there is a range of stable wavenumbers (Figures 3, 5-10). Solutions with an average wave number that is stable can also exhibit transient and periodic solutions that include double phase slips. In this regime the system can be excitable (Figure 4).

Also found in one dimension are solutions where the dynamics are chaotic and characterized by the irregular occurrence of double phase slips in both space and time (Figures 11, 12). Particularly striking are solutions in which the chaos is confined to only a part of the homogeneous system (Figures 13-15). An effective phase diffusion equation utilizing the long-term phase conservation of the solution explains the localization of this new form of amplitude chaos

(Figures 16-18).

A double phase slip in one dimension corresponds to a *bound defect pair* in two dimensions. A bound defect pair consists of two dislocations which are formed together, move apart, then move back together and annihilate each other. These bound defect pairs are prominent in our two-dimensional simulations (Figure 21).

So far we have not identified a particular physical system which exhibits the behavior described here. It is natural to suspect that the closing of the Eckhaus curve (cf. Figure 1) is related to the occurrence of double phase slips. If that should be the case, parametric driving of waves which are Benjamin-Feir unstable in the absence of any forcing should be a good candidate for this behavior. Within the framework of the coupled Ginzburg-Landau equations (1,2) these waves become unstable near the band center when forced sufficiently strongly [48]. Depending on the sign of certain nonlinear coefficients this indicates instability at all wavenumbers and a closing of the Eckhaus curve. Further work is needed to investigate the origin of the double phase slips and parameter values for which the dynamics seen in our study can be observed. Of particular interest is whether double phase slips might occur in a Faraday experiment.

Independent of experimental realizability, a very interesting theoretical question arises with regard to the bound defect pairs in two dimensions. In thermodynamic equilibrium the unbinding transition of defect pairs has been studied in great detail in the context of two-dimensional melting [49,50]. In the vicinity of that phase transition quite unusual scaling properties were found. It has been conjectured that such a transition should also be possible in nonequilibrium systems [51,52,1] but no very convincing instance has been identified so far.

The use of an effective phase diffusion equation for the large scale behavior of the chaotic state where the effective diffusion coefficient is positive but the usual phase diffusion coefficient is negative (indicating that the non-chaotic solution is unstable) is similar to studies using the Kardar-Parisi-Zhang equation [53], which is Burger's equation with a Gaussian forcing term added, to model chaotic solutions of the Kuramoto-Sivashinsky equation [54–56]. Presumably a similar noise term $\zeta(X, T)$ could be added to (13) to describe the effect of the shortscale chaotic dynamics on the effective phase,

$$\partial_T \hat{\phi} = \hat{D}_0 \partial_X^2 \hat{\phi} + \hat{D}_1 \partial_X \hat{\phi} \partial_X^2 \hat{\phi} + \zeta(X, T) + \dots \quad (29)$$

The form of the nonlinear term, which results from expanding the diffusion coefficient \hat{D} around some wavenumber \hat{q}_0 , differs from that found in the Kardar-Parisi-Zhang equation since the parametrically driven standing waves have an additional reflection symmetry as compared to the traveling waves described by the Kuramoto-Sivashinsky equation. Power counting [57] indicates that in the limit of very long scales the nonlinear terms in (29) are not relevant (neither in one nor two dimensions), in contrast to the nonlinear terms in the Kardar-Parisi-Zhang equation. A particularly interesting feature of (29) is, however, that even the effective diffusion coefficient \hat{D}_0 can become negative. This is not reported for the Kardar-Parisi-Zhang equation as applied to the Kuramoto-Sivashinsky equation. It suggests that noise may be quite important in the regime in which \hat{D} is small, i.e. near the onset of domain formation.

We would like to thank J. Eggers, G. Grinstein, and Y. Tu for stimulating discussions. This work was supported by the United States Department of Energy through grant DE-FG02-92ER14303.

- [1] M.C. Cross and P.C. Hohenberg. Pattern formation outside of equilibrium. *Rev. Mod. Phys.*, 65:851, 1993.
- [2] P. Manneville. *Dissipative Structures and Weak Turbulence*. Academic Press, Boston, 1990.
- [3] M. Golubitsky, I. Stewart, and D.G. Schaeffer. *Singularities and Groups in Bifurcation Theory*. Applied Mathematical Sciences 69. Springer, New York, 1988.
- [4] Newell A.C. and Whitehead J.A. Finite bandwidth finite amplitude convection. *J. Fluid Mech.*, 38:279, 1969.
- [5] L.A. Segel. Slow amplitude modulation of cellular convection. *J. Fluid Mech.*, 38:203, 1969.
- [6] E. N. Lorenz. Deterministic nonperiodic flow. *J. Atmosp. Sci.*, 20:130, 1963.
- [7] B.I. Shraiman, A. Pumir, W. van Saarloos, P.C. Hohenberg, H. Chaté, and M. Hofen. Spatiotemporal chaos in the one-dimensional complex Ginzburg-Landau equation. *Physica D*, 57:241, 1992.
- [8] I. Aranson, L. Kramer, and A. Weber. Core instability and spatiotemporal intermittency of spiral waves in oscillatory media. *Phys. Rev. Lett.*, 72:2316, 1994.
- [9] D.A. Egold and H.S. Greenside. Characterization of the transition from defect to phase turbulence. *Phys. Rev. Lett.*, 74:1751–1754, 1995.
- [10] H. Chaté and P. Manneville. Phase diagram of the two-dimensional complex Ginzburg-Landau equation. *Physica A*, 224:348, 1996.
- [11] P. Manneville and H. Chaté. Phase turbulence in the two-dimensional complex ginzburg-landau equation. *Physica D*, 96:30, 1996.

- [12] Y. Kuramoto. Diffusion-induced chaos in reaction systems. *Prog. Theor. Phys. Suppl.*, 64:346, 1978.
- [13] M. Faraday. On the forms and states assumed by fluids in contact with vibrating elastic surfaces. *Phil. Trans. R. Soc. Lond.*, 319, 1831.
- [14] A. Kudrolli and J.P. Gollub. Patterns and spatiotemporal chaos in parametrically forced surface waves: a systematic survey at large aspect ratio. *Physica D*, 97:133, 1996.
- [15] W.S. Edwards and S. Fauve. Patterns and quasi-patterns in the Faraday experiment. *J. Fluid Mech.*, 278:123, 1994.
- [16] S.V. Kiyashko, L.N. Korzinov, M.I. Rabinovich, and L.S. Tsimring. Rotating spirals in a Faraday experiment. *Phys. Rev. E*, 54:5037, 1996.
- [17] N.B. Tuffillaro, R. Ramshankar, and J.P. Gollub. Order-disorder transition in capillary ripples. *Phys. Rev. Lett.*, 62:422, 1989.
- [18] A. Kudrolli and J.P. Gollub. Localized spatiotemporal chaos in surface waves. *Phys. Rev. E*, 54:1052, 1996.
- [19] H. Suhl. The theory of ferromagnetic resonance at high signal powers. *J. Phys. Chem. Solids*, 1:209, 1957.
- [20] F.J. Elmer. Pattern-formation due to spin-wave instabilities - squares, hexagons, and quasi-periodic patterns. *Phys. Rev. Lett.*, 70:2028, 1993.
- [21] I. Rehberg, S. Rasenat, J. Fineberg, M. de la Torre-Juarez, and V. Steinberg. Temporal modulation of traveling waves. *Phys. Rev. Lett.*, 61:2449, 1988.
- [22] M. de la Torre-Juarez and I. Rehberg. Four-wave resonance in electrohydrodynamic convection. *Phys. Rev. A*, 42:2096–2100, 1990.
- [23] S.G.K. Tennakoon, C.D. Andereck, J.J. Hegseth, and H. Riecke. Temporal modulation of traveling waves in the flow between rotating cylinders with broken azimuthal symmetry. *Phys. Rev. E*, 54:5053, 1996.
- [24] B.W. Baxter and C.D. Andereck. Formation of dynamical domains in a circular Couette system. *Phys. Rev. Lett.*, 57:3046, 1986.
- [25] S. Ciliberto and M.A. Rubio. Local oscillations, traveling waves, and chaos in rayleigh-bénard convection. *Phys. Rev. Lett.*, 58:2652, 1987.
- [26] G.D. Granzow and H. Riecke. Phase diffusion in localized spatio-temporal amplitude chaos. *Phys. Rev. Lett.*, 77:2451, 1996.
- [27] H. Riecke, J.D. Crawford, and E. Knobloch. Time-modulated oscillatory convection. *Phys. Rev. Lett.*, 61:1942, 1988.
- [28] D. Walgraef. External forcing of spatio-temporal patterns. *Europhys. Lett.*, 7:485, 1988.
- [29] H. Riecke, J.D. Crawford, and E. Knobloch. Temporal modulation of a subcritical bifurcation to travelling waves. In P. Couillet and P. Huerre, editors, *The Geometry of Nonequilibrium*, pages 61–64. Plenum Press, 1991.
- [30] E. Knobloch and J. De Luca. Amplitude equations for travelling wave convection. *Nonlinearity*, 3:975, 1990.
- [31] E. Knobloch. Nonlocal amplitude equations. In S. Kai, editor, *Pattern Formation in Complex Dissipative Systems*. World Scientific, 1992.
- [32] R.D. Pierce and E. Knobloch. On the modulational stability of traveling and standing water waves. *Phys. Fluids*, 6:1177, 1994.
- [33] B.J. Matkowsky and V. Volpert. Coupled nonlocal complex Ginzburg-Landau equations in gasless combustion. *Physica D*, 54:203, 1992.
- [34] J.M. Vega. On the amplitude equations arising at the onset of the oscillatory instability in pattern-formation. *SIAM J. Math. Anal.*, 24:603, 1993.
- [35] H. Riecke. Stable wave-number kinks in parametrically excited standing waves. *Europhys. Lett.*, 11:213, 1990.
- [36] W. Eckhaus. *Studies in nonlinear stability theory*. Springer, New York, 1965.
- [37] T.B. Benjamin and J.E. Feir. The disintegration of wave trains on deep water. *J. Fluid Mech.*, 27:417, 1967.
- [38] L. Kramer and W. Zimmermann. On the Eckhaus instability for spatially periodic patterns. *Physica D*, 16:221, 1985.
- [39] L. Tuckerman and D. Barkley. Bifurcation analysis of the Eckhaus instability. *Physica D*, 46:57, 1990.
- [40] J. Hegseth, J.M. Vince, M. Dubois, and P. Bergé. Pattern domains in Rayleigh-Bénard slot convection. *Europhys. Lett.*, 17:413, 1992.
- [41] S. Residori, P.L. Ramazza, E. Pampaloni, S. Boccaletti, and F.T. Arecchi. Domain coexistence in 2-dimensional optical-patterns. *Phys. Rev. Lett.*, 76:1063, 1996.
- [42] D. Raitt and H. Riecke. Domain structures in fourth-order phase and Ginzburg-Landau equations. *Physica D*, 82:79–94, 1995.
- [43] D. Raitt and H. Riecke. Domain structures in Faraday waves in ferro-fluids. *Phys. Rev. E*, January, 1997.
- [44] H.R. Brand and R.J. Deissler. Confined states in phase dynamics. *Phys. Rev. Lett.*, 63:508, 1989.
- [45] T.P. Witelski. The structure of internal layers for unstable nonlinear diffusion equations. *preprint*, 1996.
- [46] M. Wu, C.D. Andereck, and H.R. Brand. The phase dynamics of turbulent Taylor vortex flow. *Europhys. Lett.*, 19:587, 1992.
- [47] M. Silber, H. Riecke, and L. Kramer. Symmetry-breaking Hopf bifurcation in anisotropic systems. *Physica D*, 61:260–278, 1992.
- [48] H. Riecke. On the stability of parametrically excited standing waves. In F.H. Busse and L. Kramer, editors, *Nonlinear Evolution of Spatio-Temporal Structures in Dissipative Continuous Systems*, pages 437–444, New York, 1990. Plenum Press.
- [49] D.R. Nelson and B.I. Halperin. Dislocation-mediated melting in two dimensions. *Phys. Rev. B*, 19:2457, 1979.

- [50] J.M. Kosterlitz and D.J. Thouless. Ordering, metastability and phase transitions in two-dimensional systems. *J. Phys. C*, 6:1181, 1973.
- [51] R. Occelli, E. Guazzelli, and J. Pantaloni. Order in convective structures. *J. Phys. Lett.*, 44:567, 1983.
- [52] D. Walgraef, G. Dewel, and P. Borckmans. Melting of 2d nonequilibrium structures at low and high constraints. *Z. Phys. B*, 48:167, 1982.
- [53] M. Kardar, G. Parisi, and Y. Zhang. Dynamic scaling of growing interfaces. *Phys. Rev. Lett.*, 56:889, 1986.
- [54] V. Yakhot. *Phys. Rev. A*, 24:642, 1981.
- [55] S. Zaleski. A stochastic model for the large scale dynamics of some fluctuating interfaces. *Physica D*, 34:427–438, 1989.
- [56] C. Jayaprakash, F. Hayot, and R. Pandit. Universal properties of the two-dimensional Kuramoto-Sivashinsky equation. *Phys. Rev. Lett.*, 71:12, 1993.
- [57] D.J. Amit. *Field theory, the renormalization group, and critical phenomena*. McGraw-Hill, New York, 1978.

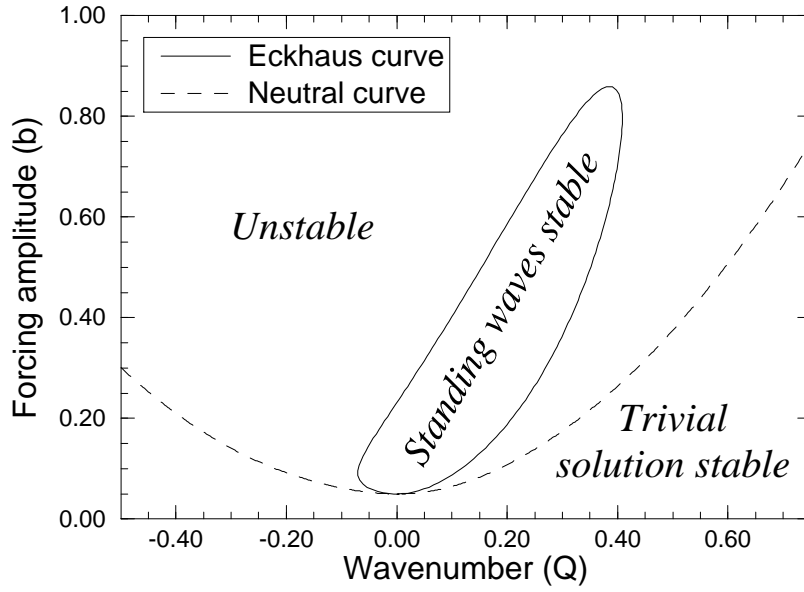


FIG. 1. Linear stability diagram for $a = -0.05$, $c = -1 + 4i$, $d = 1 + 0.5i$, $s = 0.2$, $g = -1 - 12i$.

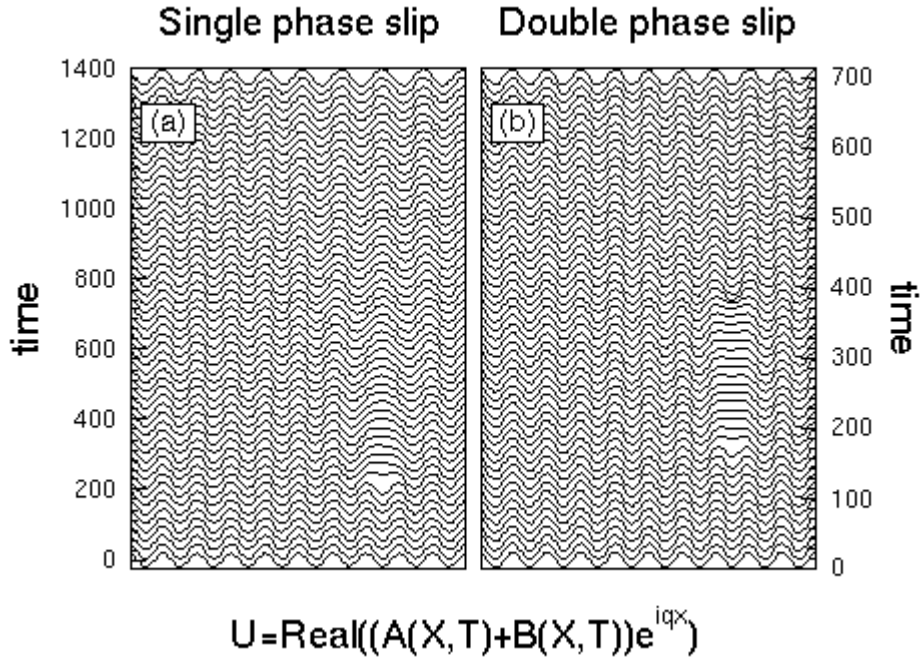


FIG. 2. Space-time diagram illustrating (a) single phase slip observed for small values of the forcing amplitude (e.g. $b = 0.1$), and (b) double phase slip observed for larger values of the forcing amplitude (e.g. $b = 0.6$).

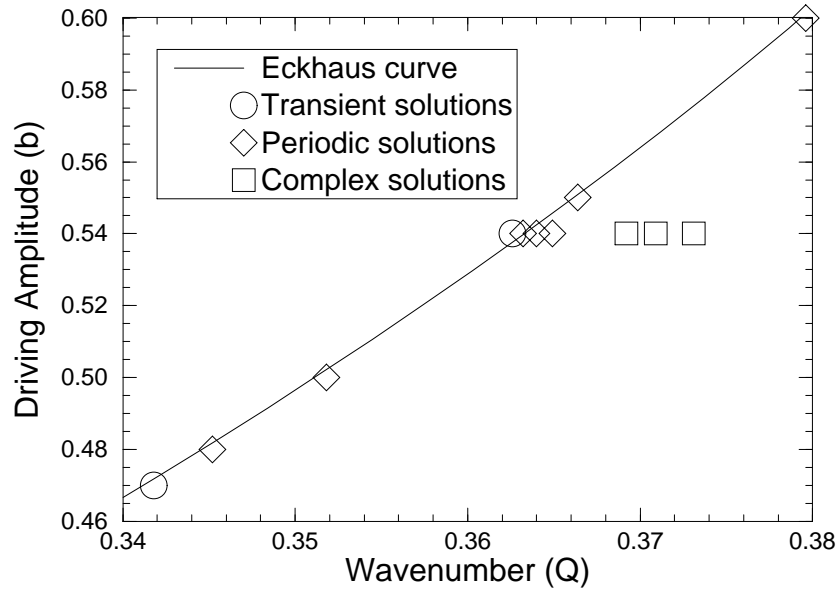


FIG. 3. Example values of the forcing amplitude b and wavenumber Q where the three solution types occur.

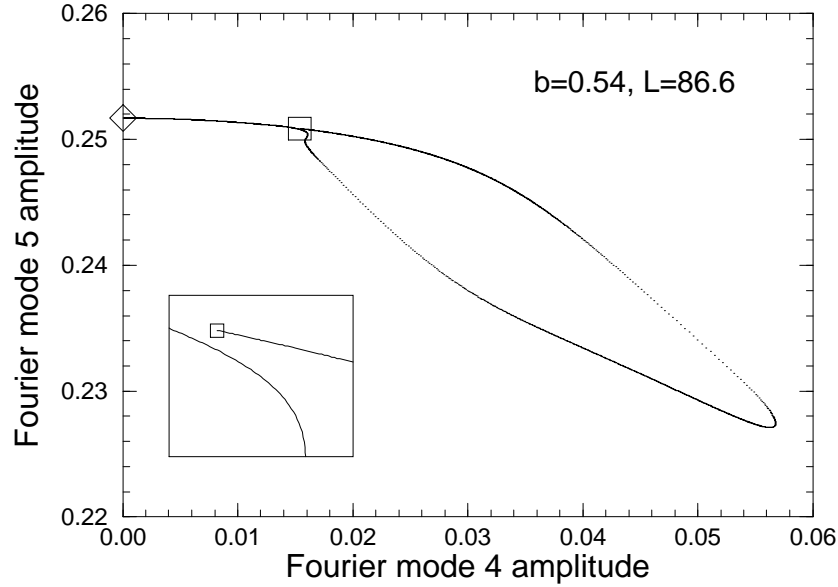


FIG. 4. Phase plane representation of a transient solution involving one double phase slip. The square indicates the initial condition which is the perturbed 5-wave state. The loop is traversed once, with the final state of the solution being the (stable) fixed point indicated by a diamond. ($b = 0.54$, $Q = 5(2\pi)/L = 0.3628$).

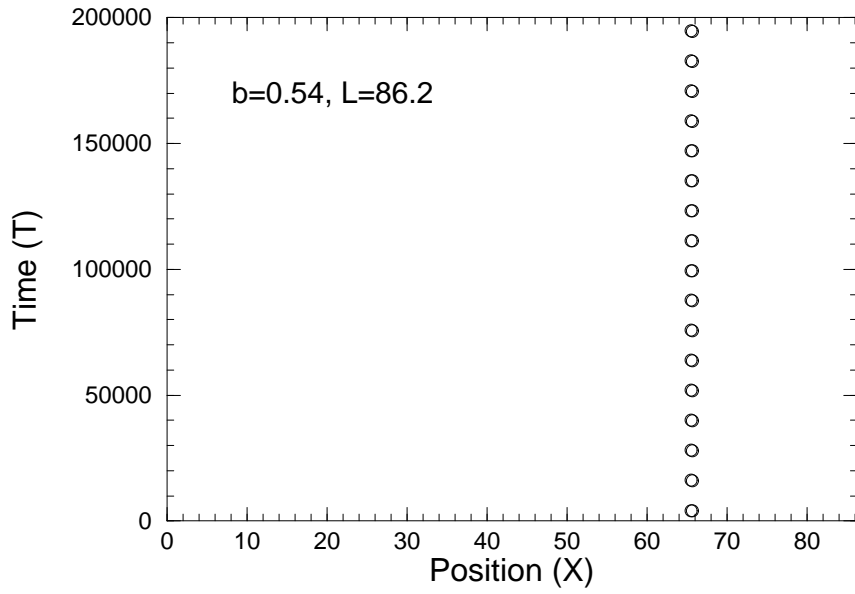


FIG. 5. Each circle represents the location (in space and time) of a double phase slip for a simple periodic solution ($b = 0.54$, $Q = 5(2\pi)/L = 0.3645$).

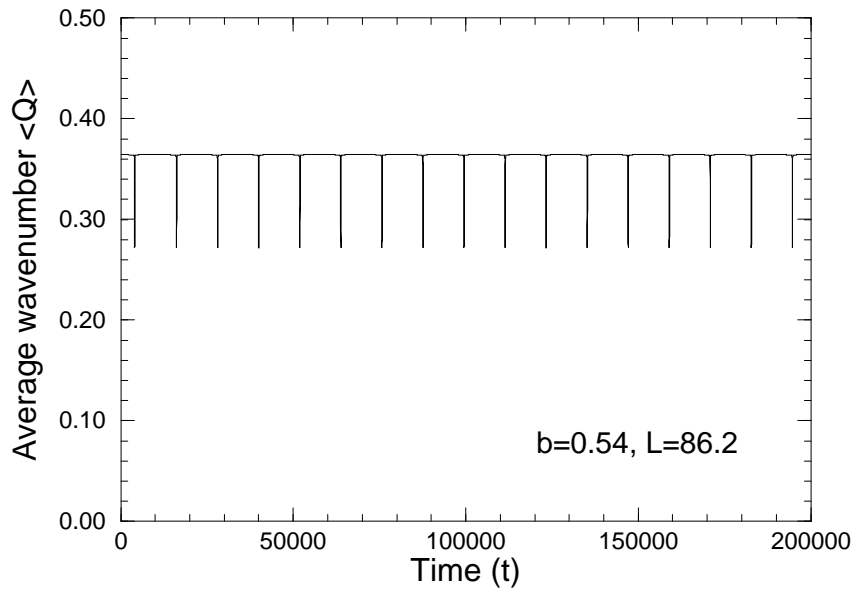


FIG. 6. Spatial average of the local wavenumber plotted as a function of time for a simple periodic solution ($b = 0.54$, $Q = 5(2\pi)/L = 0.3645$).

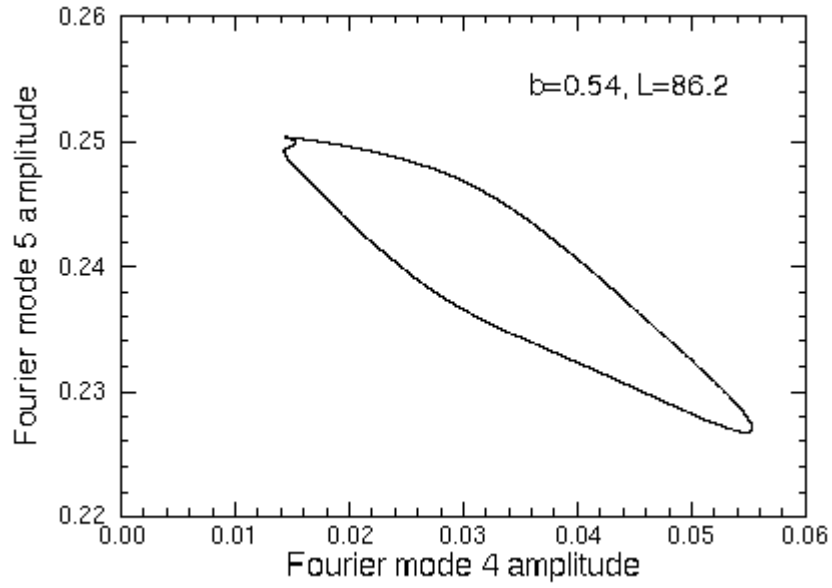


FIG. 7. Phase plane representation of a simple periodic solution ($b = 0.54$, $Q = 5(2\pi)/L = 0.3645$).

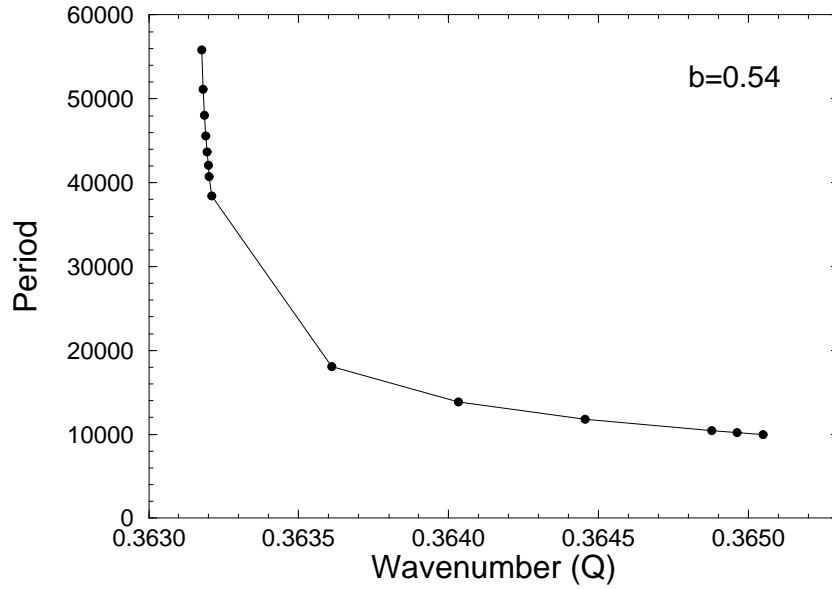


FIG. 8. Divergence of the period of the simple periodic solutions as the wavenumber Q is decreased ($b = 0.54$).

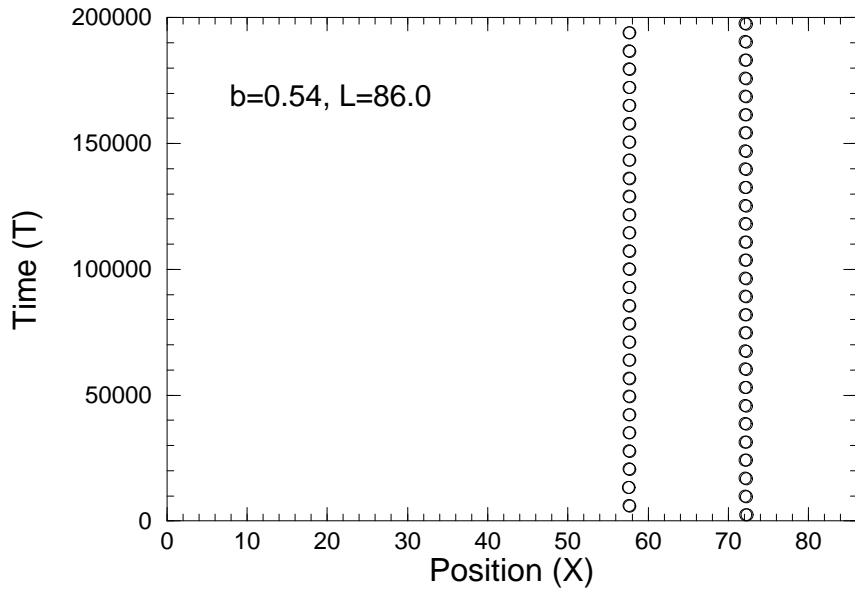


FIG. 9. Location of double phase slips for a periodic solution occurring after a period doubling bifurcation ($b = 0.54$, $Q = 5(2\pi)/L = 0.3653$).

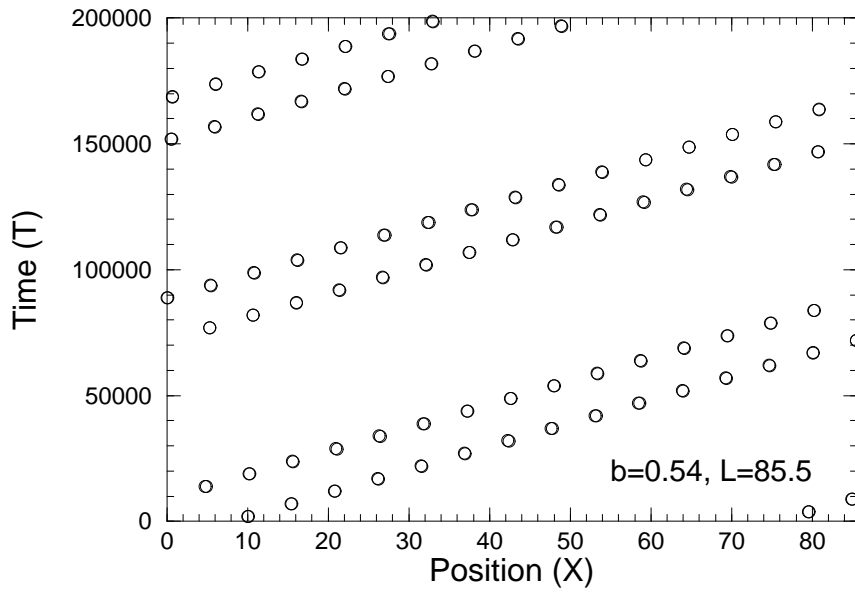


FIG. 10. Location of double phase slips for a solution where a wave of double phase slips propagates through the system ($b = 0.54$, $Q = 5(2\pi)/L = 0.3674$).

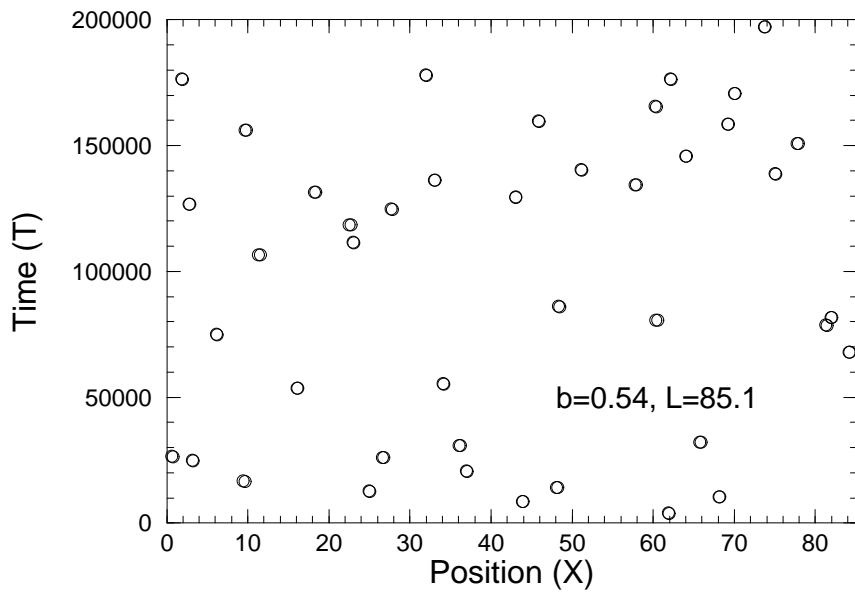


FIG. 11. A complex solution where the double phase slips occur irregularly in space and time ($b = 0.54$, $Q = 5(2\pi)/L = .3692$).

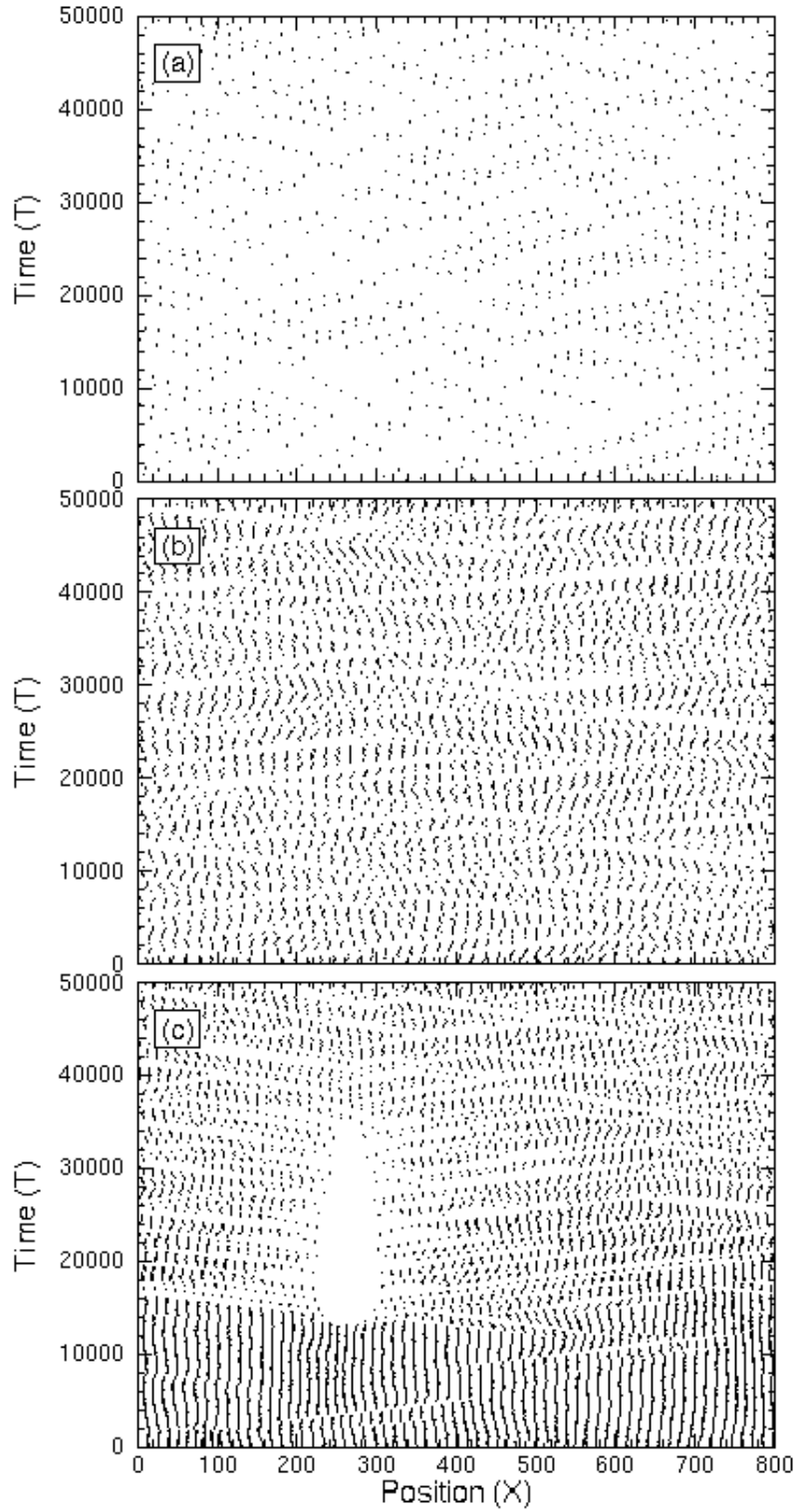


FIG. 12. Extended spatio-temporal chaos in a large system ($b = 0.6$, $L = 800$): (a) $Q = 50(2\pi)/L = 0.3927$, (b) $Q = 51(2\pi)/L = 0.4006$, (c) Initial wavenumber $Q_0 = 52(2\pi)/L = 0.4084$, after a single phase slip at $t \approx 13000$ the wavenumber is $Q = 0.4006$.

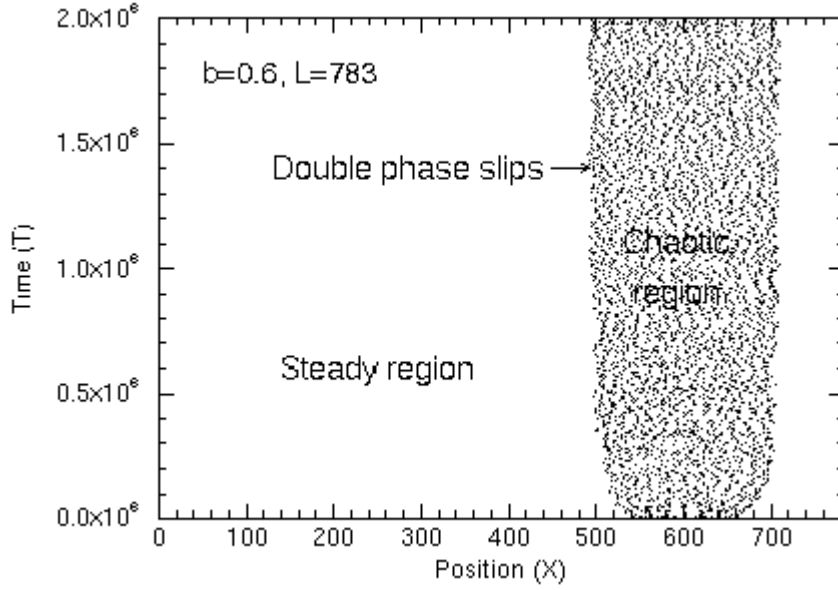


FIG. 13. Localized spatio-temporal chaos in a large domain. Each dot represents a double phase slip ($b = 0.6$, $L = 783$, $Q = 47(2\pi)/L = 0.377$).

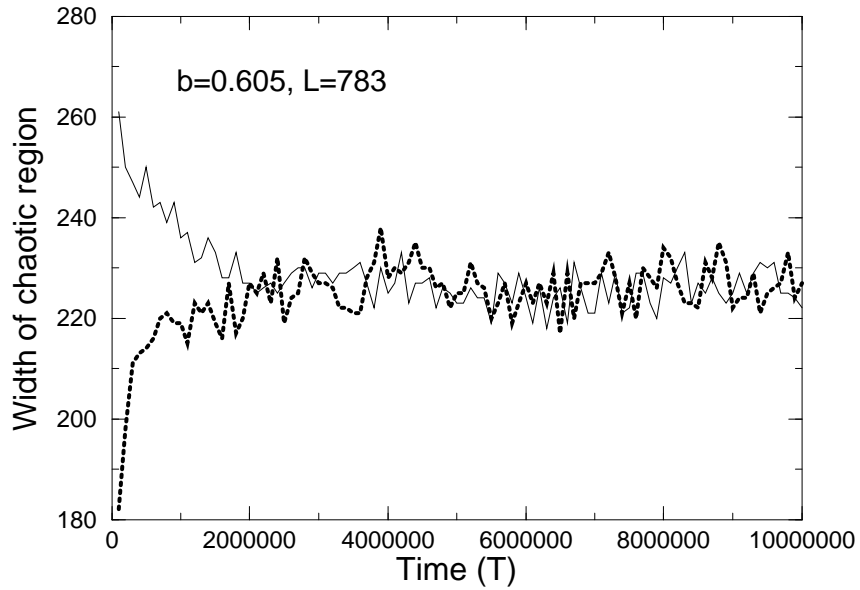


FIG. 14. Temporal evolution of the width of the localized region exhibiting spatio-temporal chaos for two different initial conditions ($b = 0.605$, $Q = 47(2\pi)/L = 0.377$).

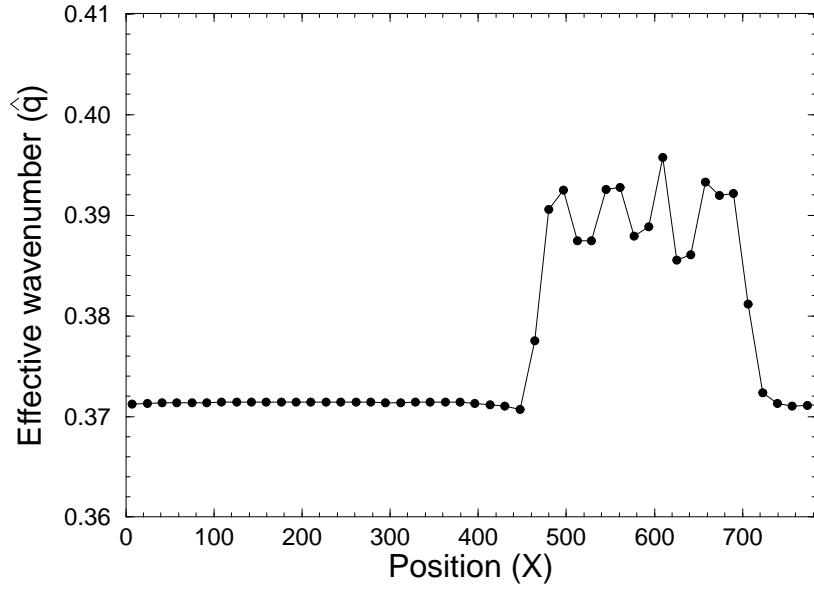


FIG. 15. Local wavenumber of the time average of $A(X, T)$ for a localized chaotic solution. The local wavenumber in the chaotic region is larger than in the quiescent region. ($b = 0.6$, $L = 783$, $Q = 47(2\pi)/L = 0.377$).

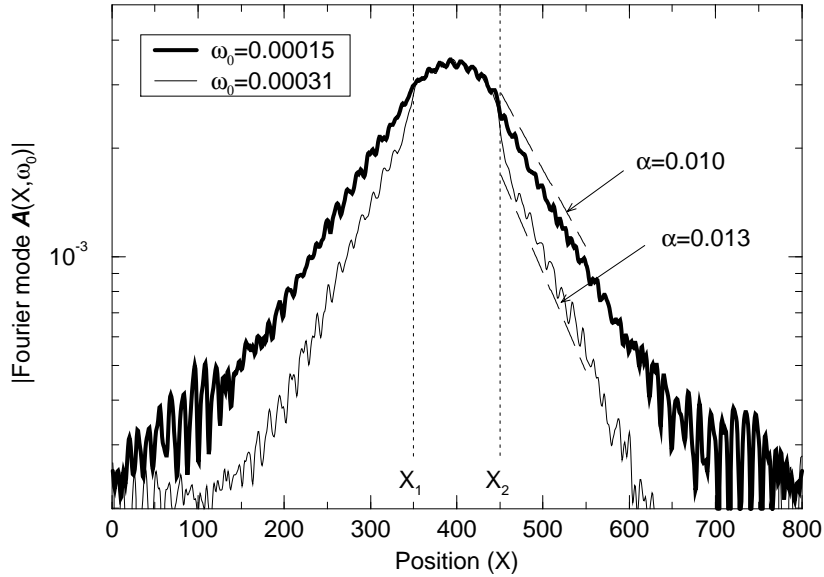


FIG. 16. Decay of the magnitude of the coefficient of the time Fourier transform of A corresponding to the frequency ω_0 in the localized advection term v in equations (14,15), for two different values of ω_0 ($b = 0.61$, $L = 800$, $Q = 51(2\pi)/L = 0.4006$, $v_0 = 1.630\omega_0$).

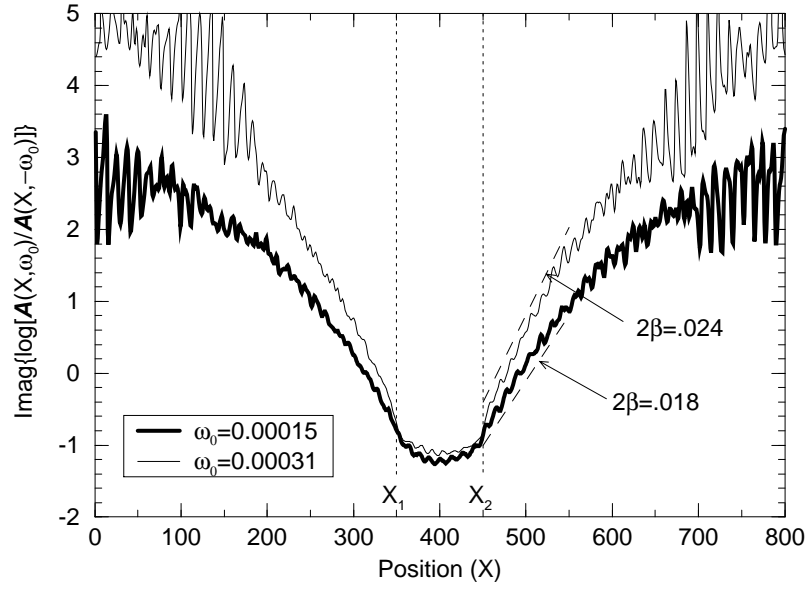


FIG. 17. Imaginary part of the ratio of the coefficients of the time Fourier transform of A corresponding to the frequencies $\pm\omega_0$ in the localized advection term v in equations (14,15), for two different values of ω_0 ($b = 0.61$, $L = 800$, $Q = 51(2\pi)/L = 0.4006$, $v_0 = 1.630\omega_0$).

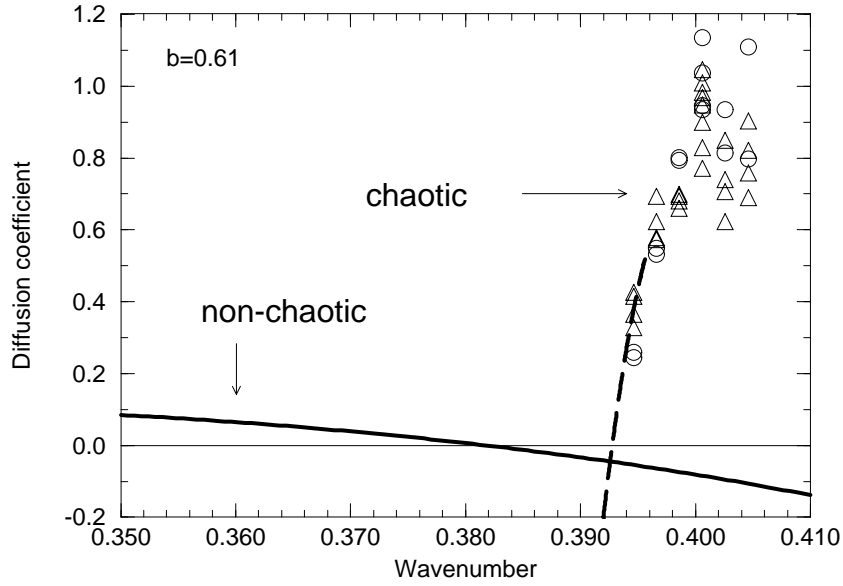


FIG. 18. Analytical phase diffusion coefficient D for the stationary solution (solid line) and effective diffusion coefficient \hat{D} for the chaotic solution; Triangles and circles represent numerical results as obtained from α and β (cf. Figures 16 and 17), the dashed line is the presumed extension of these results ($b = 0.61$).

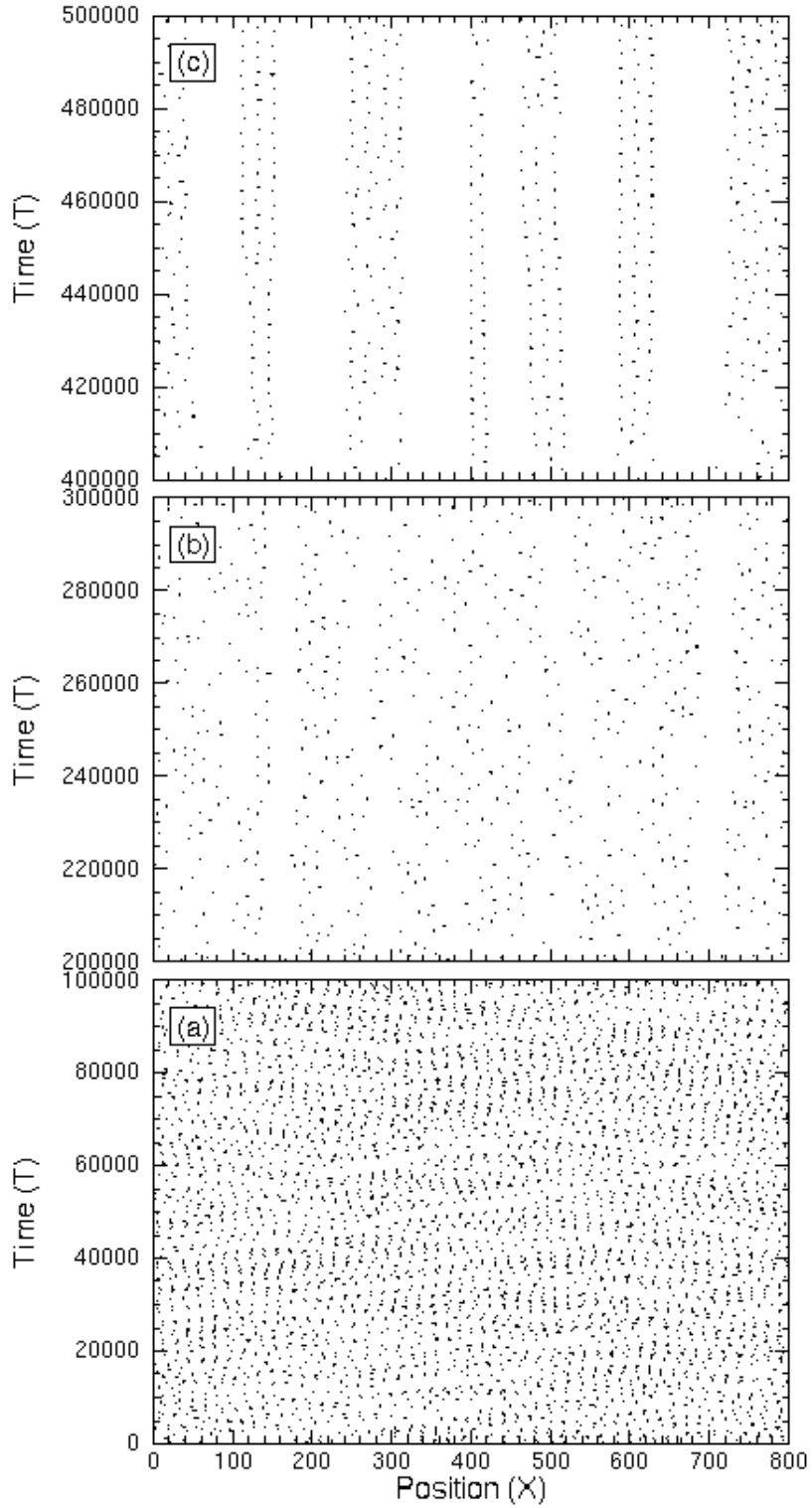


FIG. 19. A set of solutions obtained by incrementally increasing the forcing amplitude b . The extended spatio-temporal chaos breaks up into localized regions before the Eckhaus stability limit is reached ($L = 800$, $Q = 51(2\pi)/L = .4006$). (a) $b = 0.62$, (b) $b = 0.64$, (c) $b = 0.66$.

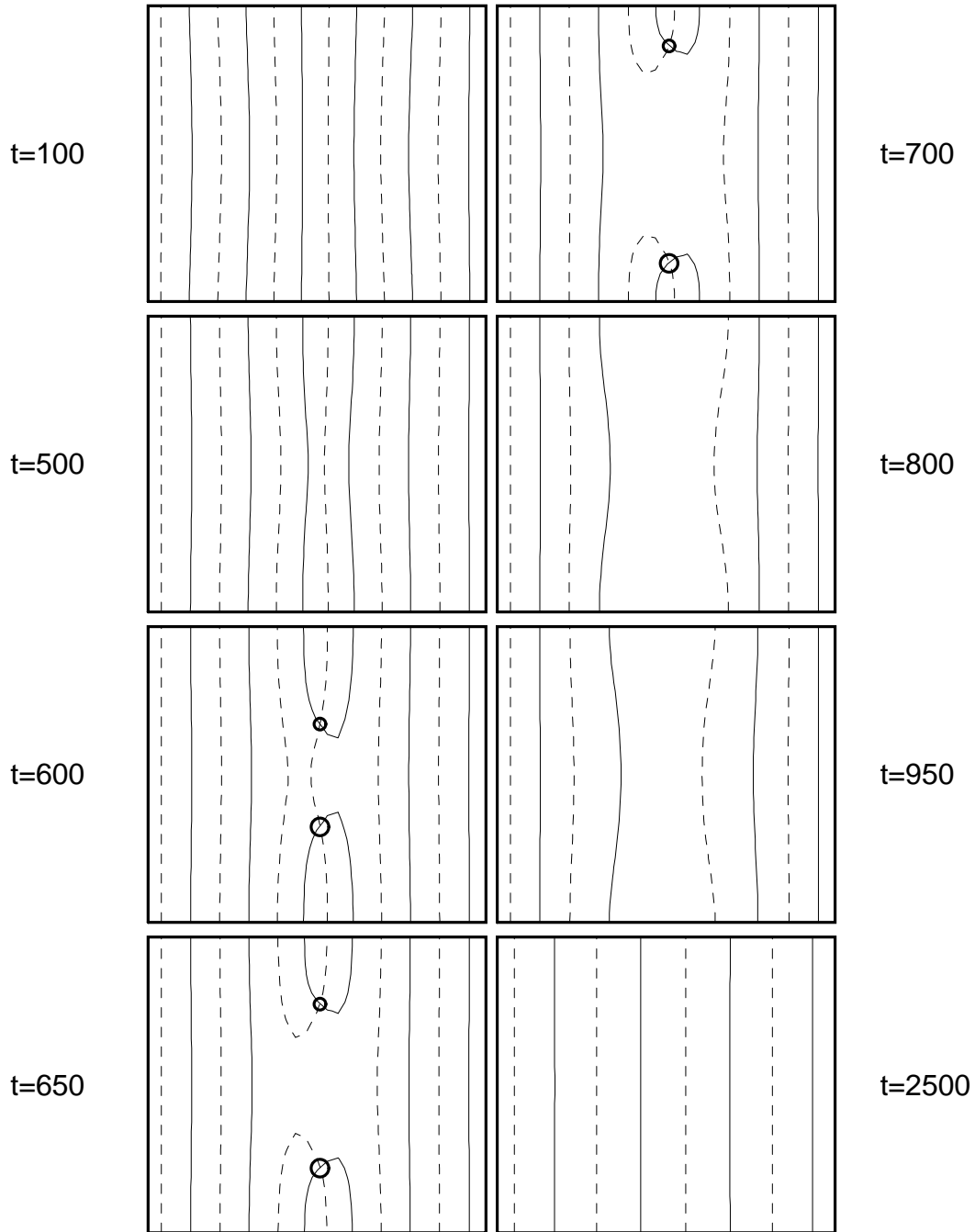


FIG. 20. Standard wavenumber reducing transition in two dimensions. Solid curves represent locations where the real part of the solution is zero. Dashed curves represent locations where the imaginary part of the solution is zero. A *bound defect pair* can be visualized by considering the left column only, progressing from the top to the bottom then returning to the top.

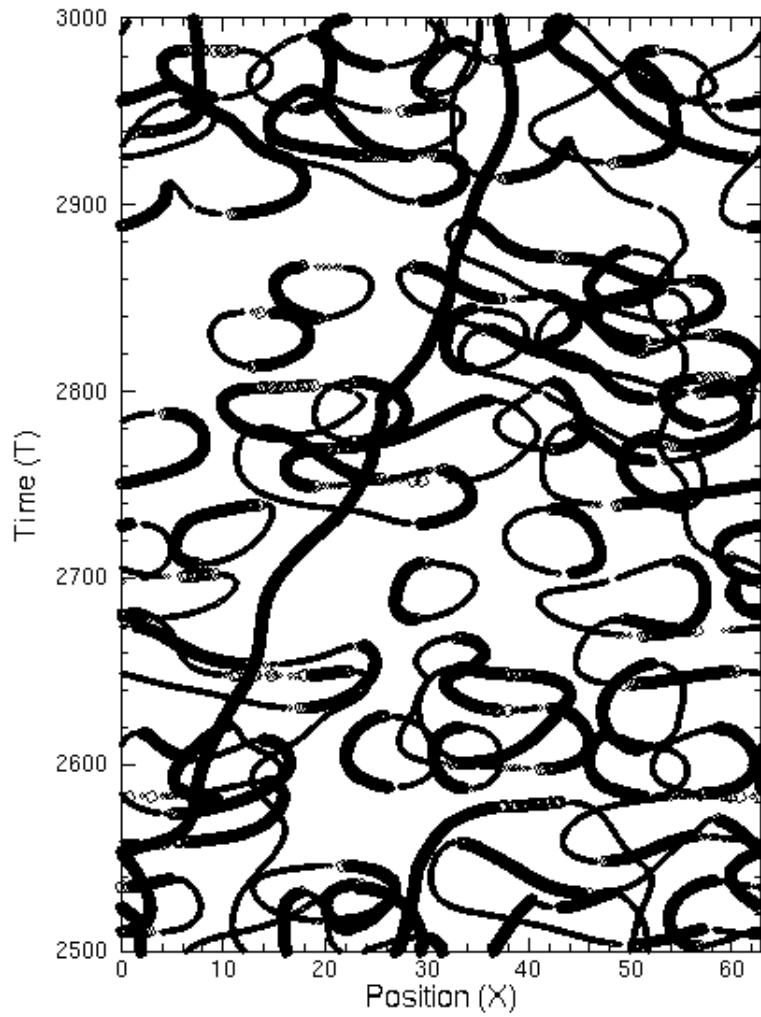


FIG. 21. Space-time diagram showing the projection of the location of defects on the x -axis for a simulation of the two-dimensional system. The *bubbles*, for example the one starting at $x \approx 29$ and $t \approx 2680$, represent bound defect pairs ($b = 1.2$, $L = 62.832$).